

# Star cluster disruption by giant molecular clouds

M. Gieles<sup>1,2</sup>, S. F. Portegies Zwart<sup>2</sup>, H. Baumgardt<sup>3</sup>, E. Athanassoula<sup>4</sup>,  
H. J. G. L. M. Lamers<sup>1,5</sup>, M. Sipior<sup>2</sup>, and J. Leenaarts<sup>1</sup>

<sup>1</sup> *Astronomical Institute, Utrecht University, Princetonplein 5, 3584 CC Utrecht, The Netherlands*

<sup>2</sup> *Astronomical Institute ‘Anton Pannekoek’, University of Amsterdam, Kruislaan 403, 1098 SJ Amsterdam, The Netherlands, Section Computational Science, University of Amsterdam, Kruislaan 403, 1098 SJ, The Netherlands*

<sup>3</sup> *Sternwarte, University of Bonn, Auf dem Hügel 71, 53121 Bonn, Germany*

<sup>4</sup> *Observatoire de Marseille, 2 Place le Verrier, 13248 Marseille Cedex 4, France*

<sup>5</sup> *SRON Laboratory for Space Research, Sorbonnelaan 2, NL-3584 CA Utrecht, The Netherlands*

Released 2006 Xxxxx XX

## ABSTRACT

We investigate encounters between giant molecular clouds (GMCs) and star clusters. We propose a single expression for the energy gain of a cluster due to an encounter with a GMC, valid for all encounter distances and GMC properties. This relation is verified with  $N$ -body simulations of cluster-GMC encounters, where the GMC is represented by a moving analytical potential. Excellent agreement is found between the simulations and the analytical work for fractional energy gains of  $\Delta E/|E_0| < 10$ , where  $|E_0|$  is the initial total cluster energy. The fractional mass loss from the cluster scales with the fractional energy gain as  $(\Delta M/M_0) = f(\Delta E/|E_0|)$ , where  $f \simeq 0.25$ . This is because a fraction  $1 - f$  of the injected energy goes to the velocities of escaping stars, that are higher than the escape velocity. We therefore suggest that the disruption time of clusters,  $t_{\text{dis}}$ , is best defined as the time needed to bring the cluster mass to zero, instead of the time needed to inject the initial cluster energy. We derive an expression for  $t_{\text{dis}}$  based on the mass loss from the simulations, taking into account the effect of gravitational focusing by the GMC. Assuming spatially homogeneous distributions of clusters and GMCs with a relative velocity dispersion of  $\sigma_{\text{cn}}$ , we find that clusters loose most of their mass in relatively close encounters with high relative velocities ( $\sim 2 \sigma_{\text{cn}}$ ). The disruption time depends on the cluster mass ( $M_c$ ) and half-mass radius ( $r_h$ ) as  $t_{\text{dis}} = 2.0 S (M_c/10^4 M_\odot) (3.75 \text{ pc}/r_h)^3 \text{ Gyr}$ , with  $S \equiv 1$  for the solar neighbourhood and  $S$  scales with the surface density of individual GMCs ( $\Sigma_n$ ) and the global GMC density ( $\rho_n$ ) as  $S \propto (\Sigma_n \rho_n)^{-1}$ . Combined with the observed relation between  $r_h$  and  $M_c$ , i.e.  $r_h \propto M_c^\lambda$ ,  $t_{\text{dis}}$  depends on  $M_c$  as  $t_{\text{dis}} \propto M_c^\gamma$ . The index  $\gamma$  is then defined as  $\gamma = 1 - 3\lambda$ . The observed shallow relation between cluster radius and mass (e.g.  $\lambda \simeq 0.1$ ), makes the value of the index  $\gamma = 0.7$  similar to that found from observations and from simulations of clusters dissolving in tidal fields ( $\gamma \simeq 0.62$ ). The constant of 2.0 Gyr, which is the disruption time of a  $10^4 M_\odot$  cluster in the solar neighbourhood, is about a factor of 3.5 shorter than found from earlier simulations of clusters dissolving under the combined effect of galactic tidal field and stellar evolution. It is somewhat higher than the observationally determined value of 1.3 Gyr. It suggests, however, that the combined effect of tidal field and encounters with GMCs can explain the lack of old open clusters in the solar neighbourhood. GMC encounters can also explain the (very) short disruption time that was observed for star clusters in the central region of M51, since there  $\rho_n$  is an order of magnitude higher than in the solar neighbourhood.

## 1 INTRODUCTION

Star clusters are subjected to various disruptive effects, which prevent low mass star clusters ( $M_c < 10^4 M_\odot$ ) from surviving for a Hubble time. From observations this was first noted by Oort (1958) and later by Wielen (1971), who showed that there is a lack of open star clusters older than a few Gyr in the solar neighbourhood. Later, more quantitative results were obtained for the life time of star clusters

(e.g. Hodge 1988 and de Grijs & Anders 2006 for clusters in the LMC; Boutloukos & Lamers 2003 for the SMC and M33; Lamers et al. 2005 and Piskunov et al. 2006 for the solar neighbourhood and Gieles et al. 2005 for the central region of M51). From the theoretical side, the evolution and disruption of star clusters has been the subject of many studies using a variety of techniques to solve the gravitational  $N$ -body problem (e.g. Ostriker, Spitzer & Chevalier 1972; Chernoff & Weinberg 1990; Gnedin & Ostriker 1997;

Takahashi & Portegies Zwart 2000; Baumgardt & Makino 2003).

Lamers, Gieles & Portegies Zwart (2005) compared observationally determined disruption times in four galaxies to the corresponding times following from the  $N$ -body simulations of clusters in tidal fields of Baumgardt & Makino (2003) and Portegies Zwart et al. (1998, 2002). They found that, based on the results of the simulations, the disruption time ( $t_{\text{dis}}$ ) should depend on the cluster mass  $M_c$  as  $t_{\text{dis}} \propto [M_c / \ln(M_c)]^{0.75} \propto M_c^{0.62}$ . The index (0.62), which is referred to as  $\gamma$ , was also determined from the observed age and mass distributions of different cluster populations (Boutloukos & Lamers 2003) and the mean value from the observations is  $\bar{\gamma} = 0.62 \pm 0.06$ . The value of  $t_{\text{dis}}$  scales with the disruption time of a  $10^4 M_\odot$  cluster as  $t_{\text{dis}} = t_4 (M_c / 10^4 M_\odot)^\gamma$ . Good agreement for  $t_4$  between simulations and observations was found only for the star clusters in the SMC. In the solar neighbourhood, the observed  $t_4$  for open clusters ( $t_4 = 1.3$  Gyr, see Lamers et al. 2005) is a factor of 5 lower than expected from the disruption time due to the galactic tidal field, combined with a realistic stellar mass function and with stellar evolution ( $t_4 = 6.9$  Gyr, see Baumgardt & Makino 2003). An even larger disagreement of almost an order of magnitude was found for  $t_{\text{dis}}$  of clusters in the central region of M51 (Gieles et al. 2005).

The fact that the observed disruption times are shorter could be a result of time-dependent external perturbations, such as spiral arm passages and encounters with giant molecular clouds (GMCs), which were ignored in the simulations of Baumgardt & Makino (2003). Terlevich (1987) and Theuns (1991) showed that a single encounter with a massive GMC could disrupt a star cluster of a few hundred  $M_\odot$  and Gieles, Athanassoula & Portegies Zwart (2006) showed that in the solar neighbourhood passages of spiral arms contribute significantly to the disruption of open clusters.

In this study we investigate the disruption of clusters by encounters with GMCs. We want to quantify whether GMCs can explain the difference between the observed values of  $t_4$  and the ones following from the simulations without the time-dependent external effects. Moreover, would simulations including encounters with GMCs preserve the numerical value of the index  $\gamma \simeq 0.62$ , where the observations and previous simulations already agree?

The paper is organised as follows: In § 2 we introduce the initial conditions for the clusters and GMCs and define the parameters involved in a cluster-GMC encounter. In § 3 we give analytical calculations of the energy gain for a cluster due to various types of encounters. These analytical formulae for the energy gain are verified with  $N$ -body simulations and compared to the mass loss of the cluster in § 4. The results of the  $N$ -body simulations are used in § 5 to derive an expression for the cluster disruption time in environments with different GMC densities. The conclusions and discussion are presented in § 6.

## 2 INITIAL CONDITIONS

### 2.1 GMC properties

In this study we consider encounters between molecular clouds and star clusters. Since 90% of the total molecular

gas mass in our Galaxy is in giant molecular clouds (GMCs) with mass  $M_n > 10^4 M_\odot$  (Solomon et al. 1987) and encounters with low mass clouds do not affect a star cluster much (e.g. Wielen 1985), we consider only the massive GMCs. In § 3 we show that the cluster energy gain due to an encounter with a GMC scales with the GMC mass squared ( $M_n^2$ ), supporting our assumption to consider only the massive clouds (i.e. the GMCs). Solomon et al. (1987) showed that there is a relation between the size and mass of galactic GMCs of

$$M_n = 540 \left( \frac{R_n}{\text{pc}} \right)^2 M_\odot, \quad (1)$$

where  $M_n$  is the mass of the GMC and  $R_n$  is its radius<sup>1</sup>. The internal density profile is of the form  $\rho(r) \propto r^{-1}$ . Eq. 1 implies a constant mean surface density of  $\Sigma_n = 170 M_\odot \text{pc}^{-2}$ .

We use the spherically symmetric Plummer model (Plummer 1911) to describe the GMC, since it is mathematically convenient to use in analytical calculations (§ 3). The potential of this model is

$$\Phi(r) = -GM / \sqrt{r^2 + a^2}, \quad (2)$$

where  $G$  is the gravitational constant,  $M$  is the total mass and  $a$  is the Plummer radius. If we choose the Plummer radius of a GMC equal to half the radius from Eq. 1, e.g.  $a_n = 0.5 R_n$ , the resulting profile is very similar to what would follow from a density profile of the form  $\rho(r) \propto r^{-1}$ . In Fig. 1 we compare the descriptions for a Plummer model (Eq. 2) and constant surface density profile (Eq. 1) for the potential in the top panel, the acceleration in the middle panel and the density profile in the bottom panel. The Plummer model has the advantage that the first derivative of the force is differentiable for each  $r$ , which is necessary for the  $N$ -body simulations.

### 2.2 Star cluster properties

For the star cluster we also choose a Plummer model (Eq. 2). The number of particles is  $N = 2048$  with a total mass of  $M_c = 1000 M_\odot$  and all stars the same mass, resulting in a realistic mean stellar mass of  $0.49 M_\odot$  (e.g. Kroupa 2001). The virial radius is set to 2 pc. For a Plummer model, the virial radius relates to the Plummer radius of the cluster as  $r_v = 16 a_c / (3\pi)$ . The cluster half-mass radius relates to  $a_c$  as  $r_h \simeq 1.305 a_c$ . Therefore, the values of  $a_c$  and  $r_h$  in physical units are 1.18 pc and 1.54 pc, respectively. The energy gain of a cluster due to an encounter with a GMC will be compared to the total initial cluster energy, e.g. the sum of kinetic and potential energy. This is defined as  $E_0 = -\eta GM_c^2 / (2r_h)$ , with  $\eta \simeq 0.4$ , depending on the cluster model. For a Plummer model  $E_0 = (3\pi/64) GM_c^2 / a_c$ , hence  $\eta \simeq 0.38$ .

### 2.3 Encounter definitions

Two particles with a relative velocity at infinity that is non-zero will experience a hyperbolic encounter. The motion of the reduced mass particle is schematically represented in

<sup>1</sup> Throughout this paper we use the subscript “ $n$ ” (from nebula or nuage) to indicate the parameters of the GMC and “ $c$ ” for the cluster.

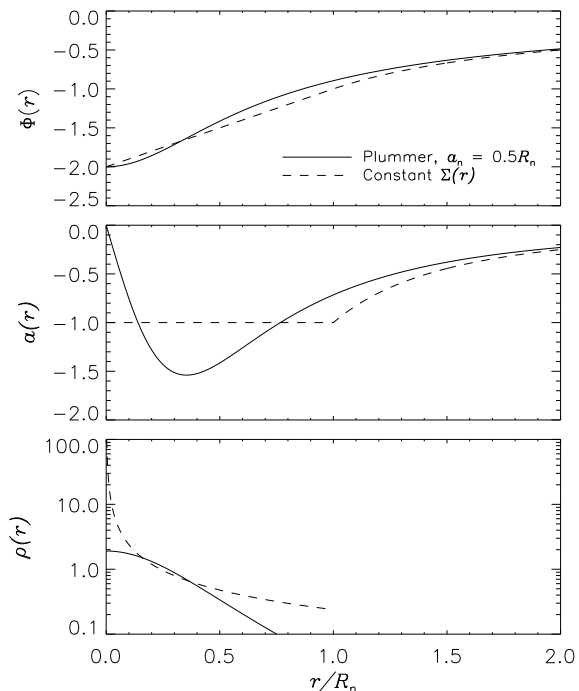


**Figure 1.** Comparison between the radial profiles of the potential (*top*), acceleration (*middle*) and density (*bottom*) for a constant surface density GMC with  $M_n = R_n = 1$ , following from Eq. 1 and  $\rho_n \propto r^{-1}$  (dashed line) and for a Plummer model with radius  $a_n = 0.5 R_n$  (full line).

Fig. 2. The impact parameter and the velocity at infinity are referred to as  $b$  and  $v_0$ , respectively. The distance of closest approach and the maximum velocity are called the encounter parameter  $p$  and  $V_{\max}$ , respectively. Conservation of angular momentum relates  $v_0$  and  $V_{\max}$  as

$$V_{\max} = v_0 \frac{b}{p}. \quad (3)$$

Consider a GMC with a Plummer model according to Eq. 2 and mass  $M_n$  and a cluster with mass  $M_c$  which is a point source. From conservation of energy and Eq. 3, it follows that  $b$  and  $p$  are related as

$$b = p \sqrt{1 + \frac{2G(M_n + M_c)}{v_0^2 \sqrt{p^2 + a_n^2}}}. \quad (4)$$

Note that  $b$  is now a mixed function of encounter and impact variables. In the next sections we will show that the encounter parameter  $p$  and  $V_{\max}$  determine the internal energy gain. Since we want to perform  $N$ -body simulations that result in an encounter with a certain desired  $p$  and  $V_{\max}$ , we use Eq. 3 and Eq. 4 to express  $p$  and  $V_{\max}$  in terms of  $b$  and  $v_0$ . In addition, in our simulations we will not start with the GMC at infinity, hence we will need to take into account the potential energy contribution at the beginning of the simulation. Since the final expressions for  $b$  and  $v_0$  as a function of  $p$ ,  $V_{\max}$ ,  $M_n$  and  $M_c$  are quite complex, but follow from simple mathematical exercises, we do not give them here.

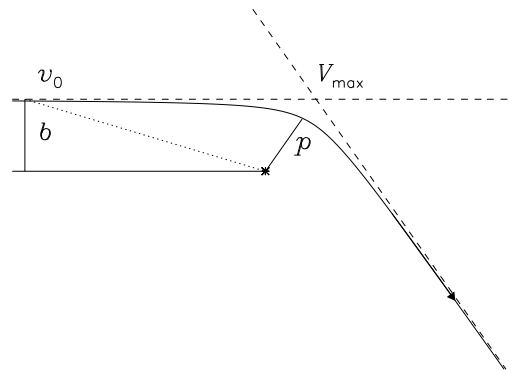


**Figure 2.** Motion of the reduced particle in a hyperbolic encounter. The impact parameter  $b$  and the velocity at infinity  $v_0$  are denoted on the left side of the picture and the encounter parameter  $p$  and maximum relative velocity  $V_{\max}$  are indicated at the point of closest approach.

There exists an analytical expression for the energy gain of a cluster due to an head-on encounter and due to a distant encounters. In the next section these relations will be extended to the full range of encounter parameters, i.e. including close encounters. The exact boundary between close and distant encounters is hard to define. Here we will distinguish three types of encounters: (1) head-on encounters for which  $p = 0$ ; (2) close encounters, where  $0 < p/a_n < 5$  and (3) distant encounters, which is for  $p \geq 5a_n$ .

### 3 CLUSTER ENERGY GAIN AND MASS LOSS DUE TO AN ENCOUNTER WITH A GMC

#### 3.1 Distant encounters

Spitzer (1958, hereafter S58) derived an expression for the energy gain of a cluster due to a distant encounter with a GMC. He assumed that the GMC is a point mass and that the encounter velocity is much faster than the internal velocity of the stars in the cluster, which is referred to as the *impulsive approximation*. The cluster energy gain can then be expressed in the encounter, GMC and cluster parameters as

$$\Delta E = \frac{1}{3} \left( \frac{2GM_n}{p^2 V_{\max}} \right)^2 M_c \bar{r}^2. \quad (5)$$

Here  $\bar{r}^2$  is the mean-square position of the stars in the cluster<sup>2</sup>.

Theuns (1991) used combined hydro-dynamical and  $N$ -body calculations of a GMC-cluster encounter, to show that Eq. 5 is very accurate. He also notes the inconvenience of the ill defined  $\bar{r}^2$  parameter. In principle  $\bar{r}^2$  follows from the cluster profile, but this variable is very sensitive to variations of the positions of stars far from the cluster centre, hence it is not constant during the simulation because of scattering

<sup>2</sup> S58 makes no distinction between  $b$ ,  $v_0$  and  $p$ ,  $V_{\max}$ . In § 4 we show that  $p$  and  $V_{\max}$  are the most convenient ones to use for calculating the energy gain.

of stars out of the cluster. Even in simulations covering a short time span,  $\bar{r}^2$  will increase due to stars that get at larger distances from the centre due to 2-body encounters in the core.

Aguilar & White (1985) have shown with  $N$ -body calculations of encounters between two Plummer models with radii  $a_1$  and  $a_2$ , that the predictions of Eq. 5 hold when  $p \geq 5 \max(a_1, a_2)$ . In § 4 we examine with  $N$ -body simulations in what regime the results of Eq. 5 are valid, and at what moment during the encounter the value for  $\bar{r}^2$  should be taken.

### 3.2 Head-on encounters

Gravitational focusing will deflect many cluster orbits which start with  $b > 5 a_n$  to encounters with  $p < 5 a_n$ , for which the relation of S58 (Eq. 5) does not hold. To obtain an expression for the energy gain for close encounters, we first explore the opposite of distant encounters, namely head-on encounters (i.e.  $p = 0$ ). In those encounters the extent of the GMC has to be taken into account, since assuming a point mass GMC would severely overestimate the energy gain. The energy gain in close encounters should be an interpolation between the distant encounter and head-on results.

Following Binney & Tremaine (1987) (Chap. 7.2, hereafter BT87) we can derive the cluster energy gain for an head-on encounter between a cluster and a GMC, both described by a Plummer model. Let  $(R, z)$  be cylindrical coordinates, with the  $z$ -axis coinciding with the GMC trajectory. Due to symmetry, the stars in the cluster get a velocity increase only perpendicular to the trajectory of the GMC, of size

$$\Delta v(R) = -\frac{2GM_n R}{V_{\max}(R^2 + a_n^2)}, \quad (6)$$

where analogous to the case of the distant encounters we use  $V_{\max}$  for the relative velocity between the cluster and the GMC. Eq. 6 can be used to calculate the energy gain of the cluster:

$$\Delta E = \pi \int_0^\infty [\Delta v(R)]^2 \Sigma(R) R dR. \quad (7)$$

Here  $\Sigma(R)$  is the surface density of the cluster obtained by projecting parallel to the line of motion of the GMC. Since the cluster is described by a Plummer model,  $\Sigma(R)$  is

$$\Sigma(R) = \frac{M_c a_c^2}{\pi} (R^2 + a_c^2)^{-2}, \quad (8)$$

so the energy gain of the cluster due to an encounter between two Plummer models is

$$\Delta E = \left( \frac{2GM_n a_c}{V_{\max}} \right)^2 M_c \int_0^\infty \frac{R^3}{(R^2 + a_n^2)^2 (R^2 + a_c^2)^2} dR. \quad (9)$$

The result of the integration is a function of  $a_c$  and  $a_n$  and is equal to  $1/12a^4$  when  $a_n = a_c = a$ . In that case, Eq. 9 reduces to the result found by BT87:

$$\Delta E_{\text{BT}} = \frac{1}{3} \left( \frac{GM_n}{V_{\max} a} \right)^2 M_c. \quad (10)$$

When  $a_n \neq a_c$ , the result of the integration is a function of  $a_c$  and  $a_n$ . Introducing a new variable  $\chi \equiv a_n/a_c$ , the ratio of the GMC and cluster radii, Eq. 9 can be written as

$$\Delta E = \frac{1}{3} \left( \frac{GM_n}{V_{\max} a_c} \right)^2 M_c \frac{12(\chi^2 - 1) - 6(\chi^2 + 1) \ln(\chi^2)}{(1 - \chi^2)^3}, \quad (11)$$

where in the first factor we recognise the result for  $a_c = a_n$  (e.g. Eq. 10) and the rest is a correction factor  $C(\chi)$  which is only a function of  $\chi$ . We can write a more general expression for the energy gain of head-on encounters

$$\Delta E = \Delta E_{\text{BT}} C(\chi), \quad (12)$$

with

$$C(\chi) = \begin{cases} \frac{12(\chi^2 - 1) - 6(\chi^2 + 1) \ln(\chi^2)}{(1 - \chi^2)^3} & \text{for } \chi \neq 1 \\ 1 & \text{for } \chi = 1 \end{cases} \quad (13)$$

The expression for  $C(\chi)$  is rather complicated, but for realistic values of  $\chi$  (i.e.  $2 < \chi < 10$ ),  $C(\chi)$  can be approximated with high accuracy by  $C(\chi) \simeq 2\chi^{-3}$  (see Fig. 4).

With Eq. 12 and Eq. 13 we have a general expression for the energy gain of head-on GMC-cluster encounters, when both are described by Plummer models, valid for any radius and mass of the cluster and the GMC. In § 4.3 we will confront Eq. 12 and Eq. 13 with results from  $N$ -body simulations.

### 3.3 A general expression for the cluster energy gain

The energy gain for a close encounter, i.e. an encounter for which the cluster moves through the cloud within a few  $a_n$  from the GMC centre, should be a smooth interpolation between the result for a head-on (Eq. 12) and distant encounters (Eq. 5). When replacing  $4\bar{r}^2/p^4$  in Eq. 5 by  $C(\chi)/a_c^2$ , we get the result for head-on encounter (Eq. 12). One way of connecting the two is to add a term in the denominator of Eq. 5, preventing the result to diverge to infinity at  $p = 0$ , so that it converges to Eq. 12, is

$$\Delta E = \frac{1}{3} \frac{4\bar{r}^2}{\left( p^2 + \sqrt{4\bar{r}^2 a_c^2 / C(\chi)} \right)^2} \left( \frac{GM_n}{V_{\max}} \right)^2 M_c. \quad (14)$$

If we use the approximation given in § 3.2 for  $C(\chi)$  (i.e.  $C(\chi) \simeq 2\chi^{-3}$ ) and the fact that  $\sqrt{r^2} \simeq 1.8 r_h$ ,  $a_c \simeq r_h/1.305$  and the real GMC radius  $R_n$  relates to  $a_n$  as  $R_n = 2a_n$ , we can rewrite Eq. 14 as

$$\Delta E \simeq \frac{4.4 r_h^2}{\left( p^2 + \sqrt{r_h R_n^3} \right)^2} \left( \frac{GM_n}{V_{\max}} \right)^2 M_c. \quad (15)$$

In the next section, this relation will be compared to results of  $N$ -body simulations for encounters with  $p$  ranging from 0 to  $10 a_n$ .

## 4 VALIDATION WITH $N$ -BODY SIMULATIONS

### 4.1 Description of the code

The  $N$ -body calculations were carried out by the *kira* integrator, which is part of the Starlab software environment (McMillan & Hut 1996; Portegies Zwart et al. 2001). *Kira* uses a fourth-order Hermite scheme and includes special

treatments of close two-body and multiple encounters of arbitrary complexity. The special purpose GRAPE-6 systems (Makino et al. 2003) of the University of Amsterdam are used to accelerate the calculation of gravitational forces between stars.

The potential, acceleration and jerk of the stars due to the GMCs are derived from Eq. 2 and calculated for each star individually, based on its position and velocity with respect to the GMC. We assume the GMCs are moving potentials which do not interact. Indeed, we are interested in the star cluster and since we consider GMCs that are  $\sim 100 - 1000$  times more massive than the cluster, the gravitational pull from the star cluster on the GMCs is negligible and will therefore not affect its orbit. Although GMCs have finite life times ( $\simeq 10 - 30$  Myr), the encounter durations are sufficiently small ( $\simeq 1$  Myr) to not be affected by this.

## 4.2 Description of the runs

We want to avoid sudden jumps in the contribution of the GMC to the cluster potential energy at the beginning and at the end of the simulations. In principle, our GMC should start at infinity, have an encounter with the star cluster and then continue until infinity. Since we do not want to evolve the cluster to long before the encounter, to restrict simulation time and to avoid too much internal dynamical evolution, we put the GMC initially at a distance of  $D = 500 a_c$  from the cluster and give it zero mass. While the GMC travels from  $D$  to  $0.9D$ , approaching the cluster, we increase its mass gradually from 0 to  $M_n$ . Similarly, after the encounter and while the GMC travels from  $0.9D$  to  $D$  we decrease its mass gradually from  $M_n$  to 0. To give the cluster time to get back to equilibrium and to give stars with velocities higher than the escape velocity time to leave the cluster we evolve it further for a time equal to half that elapsed after the encounter.

To test the different analytical expressions of § 3 for the energy gain of the cluster, we perform series of head-on ( $p = 0$ ), distant ( $p > a_n$ ) and close encounters with different GMC radii and encounter parameters. The initial velocity ( $v_0$ ) and impact parameter ( $b$ ) of the GMC are calculated from the desired values of  $p$  and  $V_{\max}$ , using the expressions for gravitational focusing of § 2.3. The cluster properties are described in § 2.2. A summary of all runs is given in Table 1. The results will be discussed in § 4.3-4.5.

All clusters are scaled to  $N$ -body units, such that  $G = M = 1$  and  $E_0 = -0.25$ , following Heggie & Mathieu (1986). Then  $r_v$  is the unit of length and follows from the scaling of the energy, since  $r_v \equiv GM_c/(4|E_0|) = 1$ , where  $E_0$  is the total (potential and kinetic) initial energy of the cluster. We assume virial equilibrium at the start of the simulation, which implies  $r_v(t = 0) = 1$ .

## 4.3 Head-on encounters

We perform  $N$ -body simulations of head-on encounters between a cluster and a GMC, both described by a Plummer model. GMCs with different Plummer radii  $a_n$  were used to compare simulations to the analytical result of Eq. 12.

The energy gain of the cluster<sup>3</sup> is always expressed in units of the initial cluster energy, i.e. the fractional energy gain ( $\Delta E/|E_0|$ ). Since we are here interested in the effect of the GMC radius on  $\Delta E/|E_0|$ , we fix the mass of the GMC at a constant value. The results can then be compared with the predicted value from Eq. 12. More specific, when we divide the energy gain for the different cases by the value that was predicted by BT98 (e.g. Eq. 10), we should get the factor  $C(\chi)$  of Eq. 13. In § 4.5 we show that there is no good agreement between the simulations and the analytical predictions when  $\Delta E/|E_0| \gg 1$ . To keep  $\Delta E/|E_0| < 1$  for all GMC radii, we choose  $M_n = 10^4 M_\odot$ , which is somewhat lower than a realistic value for  $M_n$ . We choose integer values for  $\chi$  from 1 to 10, where Eq. 10 and Eq. 12 should be valid for  $\chi = 1$  and  $\chi \neq 1$ , respectively. The encounter velocity for all simulations is  $V_{\max} = 20 \sigma_{\text{rms}}$ , where  $\sigma_{\text{rms}} = 1 \text{ km s}^{-1}$  is the internal velocity dispersion of stars in the cluster.

In Fig. 4 we show the results of  $\Delta E/|E_0|$  from the  $N$ -body simulations for different  $\chi$  with diamond symbols, the value of BT87 with a filled circle (left) and the result of Eq. 12 with the full line. The latter relation is also shown with a dashed line, but with an approximation for  $C(\chi)$  of the form  $C(\chi) = 2\chi^{-3}$ . This approximation is very close to the real  $C(\chi)$  for  $2 \leq \chi \leq 9$ . Excellent agreement between the analytical work and the  $N$ -body results is found in all cases.

In Fig. 3 we show snapshots of a cluster during a head-on encounter with a GMC. In the top panels the line of sight is perpendicular to the trajectory of the GMC, whose direction is parallel to the  $x$ -axis. The attractive force of the GMC parallel to its trajectory before and after the encounter cancel out, resulting in displacement of stars only perpendicular to the line of motion of the GMC. In the bottom panels the line of sight is along the motion of the GMC, and it can be seen that the stars escape and form a disk like structure of unbound particles around the cluster. The time with respect to the encounter moment is indicated in each panel in the top row, in units of  $t_{\text{enc}}$ , where  $t_{\text{enc}} \equiv 2a_n/V_{\max}$ .

## 4.4 Distant and close encounters

For the simulations of distant encounters we choose  $M_n = 10^5 M_\odot$ . The tidal forces of the GMC deform the cluster into a cigar like shape, as can be seen in Fig. 6. In Fig. 5 we show with the full lines the evolution of the internal energy of the cluster for encounters with three different values for  $p$  as a function of time, in units of the encounter time ( $t_{\text{enc}} \equiv p/V_{\max}$ ). (Note that for head-on encounters  $t_{\text{enc}} \equiv 2a_n/V_{\max}$ .) We define time ( $t$ ) such that the moment of closest approach is at  $t = 0$ . The value of  $V_{\max}$  for these runs is  $40 \sigma_{\text{rms}}$  and the GMC radius is equal to the cluster radius. The GMC radius is chosen small in this example in order not to have too large values of  $p$  when the ratio  $p/a_n$  is large. Otherwise, the energy gain would be too small. The results of Eq. 5 for these encounters are overplotted as the

<sup>3</sup> We start the cluster in the origin, resulting in a centre of mass velocity after the passage of the GMC. In the comparison with the analytical models, when we refer to cluster energy, we refer to the sum of the *internal* potential and *internal* kinetic energy, i.e. the energy after the centre of mass motion has been subtracted.

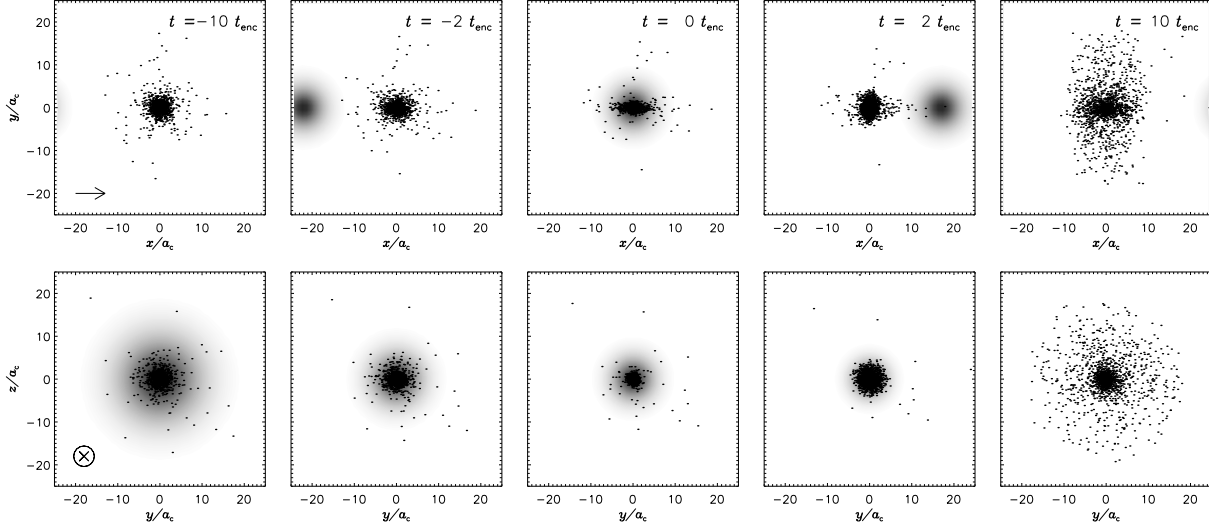


**Figure 3.** Snapshots of a star cluster undergoing a head-on encounter with a GMC of  $M_n = 10^4 M_\odot$  with  $V_{\max} = 20 \sigma_{\text{rms}}$ . The motion of the GMC is along the  $x$ -axis the line of sight is perpendicular to (*top panels*) and along (*bottom panels*) the GMC trajectory. The arrows in the left lower corner of the left panels are parallel to the direction of motion of the GMC. The GMC is shown with grey shades based on the surface density of a GMC with  $a_n = 5.8 a_c$ . The time with respect to the moment of encounter is indicated in each panel of the top row, where  $t_{\text{enc}} \equiv 2a_n/V_{\max}$ . The snapshots are taken in the centre-of-mass frame of the cluster and the viewing distance is  $40 a_c$ .

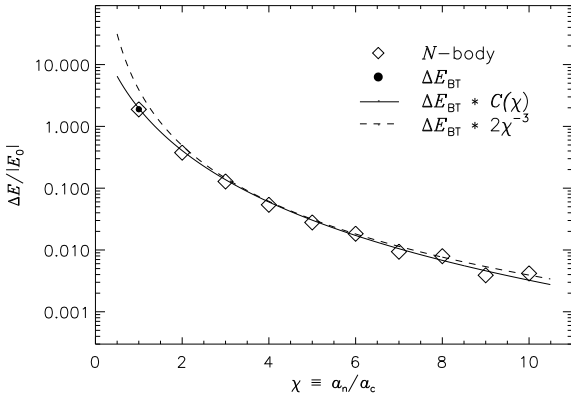


**Figure 4.** Fractional energy gain ( $\Delta E/|E_0|$ ) for a star cluster due to head-on encounters with GMCs with  $M_n = 10^4 M_\odot$  for different  $\chi \equiv a_n/a_c$  and with  $V_{\max} = 20 \sigma_{\text{rms}}$ . The analytical approximation of BT87 (Eq. 10) for head-on encounters between identical Plummer models is indicated with a filled circle (left). The  $N$ -body results are shown with diamonds. The analytical prediction of Eq. 12 with the correction factor  $C(\chi)$  for different cloud radii is shown with the full line. The predicted energy gain with an approximation for  $C(\chi)$  (i.e.  $C(\chi) = 2\chi^{-3}$ ) is shown with the dashed line.

dashed lines. The value of  $\bar{r}^2$  changes during the simulations due to internal dynamical effects and because of deformation of the cluster by the GMC. This last effect is clearly visible in Figs. 3 and 6. Since the result of Eq. 5 is very sensitive to the value of  $\bar{r}^2$ , we performed tests to find at which time  $\bar{r}^2$  should be taken to get the best agreement between Eq. 5 and the simulations. If we take this value too early, Eq. 5 will underestimate the energy gain compared to the

result of the simulation. This because dynamical evolution will increase  $\bar{r}^2$ . When using a value  $\bar{r}^2$  which is determined during the encounter (i.e.  $t \simeq 0$ ), the energy gain from Eq. 5 overestimates the true value. We found that best agreement was found when using  $\bar{r}^2$  at  $t = -2 t_{\text{enc}}$ . From Fig. 5 it can be seen that this is moment where the energy of the cluster starts to increase, whereas the cluster energy is almost constant before that moment.

The variations of the relative velocity between the cluster and the GMC are smaller than the variations in  $\bar{r}^2$ , and for that reason the result of Eq. 5 is less sensitive to the time that we choose the velocity. Since most of the energy is injected between  $-t_{\text{enc}}$  and  $+t_{\text{enc}}$  (Fig. 5), the best agreement is obtained when the relative velocity at  $t = 0$ , e.g.  $V_{\max}$ , is used.

To test the validity of the interpolation between the distant and the head-on encounters (Eq. 14), we performed  $N$ -body simulations of various encounters with impact parameter  $p$  ranging from 0 to 10 times the GMC radius  $a_n$ . The encounter velocity was chosen  $40 \sigma_{\text{rms}}$ , such that the fractional energy gain is always lower than 1 (Eq. 12). The impact parameter  $b$  and initial velocity  $v_0$  of the GMC were calculated using Eq. 4. The GMC mass is  $10^5 M_\odot$  and we used the observed mass-radius relation for GMCs (Eq. 1), resulting in  $\chi = 5.8$  and therefore  $C(\chi) = 0.01$  (Eq. 13). In Fig. 7 we show the result of  $\Delta E/|E_0|$  from the  $N$ -body simulations (diamonds) and the analytical prediction of Eq. 14 (full line). The predictions for the two extreme values of  $p$ , i.e. for distant and for head-on encounters are shown with the dashed line and the filled circle (left), respectively. The analytical expression Eq. 14 agrees very well with the results from the  $N$ -body simulations. It can be seen that the prediction of S58 is accurate for  $p \geq 5 a_n$ , in agreement with what was found by Aguilar & White (1985). Note that in

**Table 1.** Summary of the  $N$ -body simulations. All runs mentioned are done 4 times and average results are used. (1) GMC mass in units of  $M_c = 10^3 M_\odot$ ; (2) ratio of the GMC radius and cluster radius ( $\chi = a_n/a_c$ , where  $a_c=1.18$  pc); (3) impact parameter in units of GMC radius; (4) impact velocity in units of internal cluster velocity dispersion ( $\sigma_{\text{rms}}$ ); (5) and (6) are the encounter distance and velocity, following from columns (3),(4) and Eq. 4 and Eq. 3; (7) Figure numbers where the results of the runs are shown.

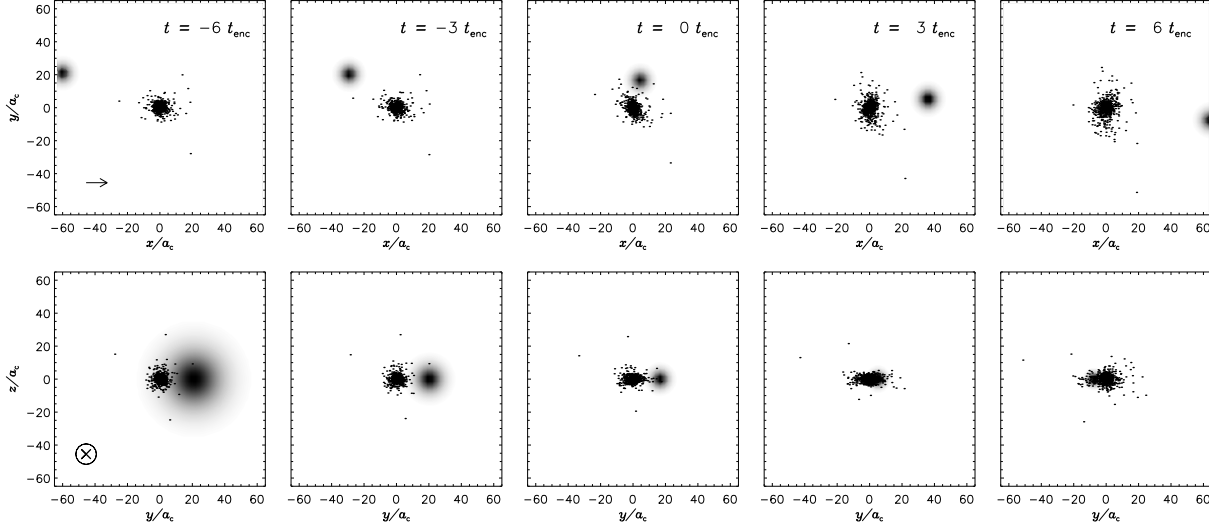
(1) $M_n/M_c$	(2) $\chi$	(3) $b/a_n$	(4) $v_0/\sigma_{\text{rms}}$	(5) $p/a_n$	(6) $V_{\text{max}}/\sigma_{\text{rms}}$	(7) Figure
10	1	0	17.9	0	20	4
	2	0	19.0	0	20	
	3	0	19.3	0	20	
	4	0	19.5	0	20	
	5	0	19.6	0	20	
	6	0	19.7	0	20	
	7	0	19.7	0	20	
	8	0	19.8	0	20	
	9	0	19.8	0	20	
	10	0	19.8	0	20	
200	1	10.8	27.7	10	30	5
		15.8	28.5	15	30	
		20.8	28.9	20	30	
10	5.8	0	19.6	0	20	3
100	5.8	3.3	14.2	3	15	6
100	5.8	0	38.44	0	40	7,8,10,9
		0	16.67	0	20	
		0	4.67	0	10	
		0.324	38.52	0.3125	40	
		0.371	16.85	0.3125	20	
		0.708	5.30	0.3125	10	
		0.645	38.74	0.625	40	
		0.720	17.35	0.625	20	
		1.117	6.72	0.625	10	
		1.278	39.14	1.25	40	
		1.372	18.22	1.25	20	
		1.722	8.71	1.25	10	
		2.530	39.52	2.5	40	
		2.628	19.03	2.5	20	
		2.914	9.09	2.5	10	
		5.030	39.76	5	40	
		5.122	19.53	5	20	
		5.361	9.19	5	10	
		10.026	39.89	10	40	
		10.107	19.79	10	20	
		10.306	9.64	10	10	

Fig. 7 we have used  $a_n$  as a scale length to normalise  $p$ . This is possible since GMCs have finite sizes. If we were dealing with objects of infinitesimal size, as e.g. black holes, this scaling would not be possible. Thus, Fig. 7 can not be applied to those cases. For large  $p$  ( $p \gg a_n$ ) the energy gain only depends on  $p$ . This is demonstrated by the good agreement with the point source approximation of S58, since for these cases  $a_n = 0$ .

To see if the agreement between our predicted energy gain from Eq. 14 and  $N$ -body simulations holds for lower velocities, we performed a similar series  $N$ -body simulations as shown in Fig. 7 for  $V_{\text{max}} = 10\sigma_{\text{rms}}$  and  $20\sigma_{\text{rms}}$ . The values of  $\Delta E/|E_0|$  for these three different values of  $V_{\text{max}}$  and different values of  $p$  is shown in Fig. 8. For the lower velocities we again find very good agreement. However, when the fractional energy gain is larger than 1, the  $N$ -body simulations show a smaller energy gain than the predictions. The dif-

ference is larger for larger energy gains. Similar results were obtained by Gieles et al. (2006) for one-dimensional shocks due to spiral arms. This is probably because the impulsive approximation does not hold anymore. When the GMC is very massive, or when the relative velocity is low, the stars in the cluster are displaced too much before the encounter. The symmetry assumption of the encounter of the impulse approximation then does not hold anymore.

The energy gain from the encounter is absorbed mainly by the stars far from the cluster centre, which can gain velocities much higher than the escape velocity. A bound core will remain, even when  $\Delta E/|E_0| \gg 1$ . Both topics will be discussed in more detail in § 4.5.



**Figure 6.** Snapshot of a star cluster during a distant encounter with a GMC with  $M_n = 100 M_c$ ,  $p = 3 a_n$  and  $V_{\max} = 15 \sigma_{\text{rms}}$  in the centre of mass frame of the cluster. The motion of the GMC is along the  $x$ -axis, starting at  $b = y = 20 a_c$ , and the line of sight is perpendicular to (*top panels*) and along (*bottom panels*) the GMC trajectory. The arrows in the left lower corner of the left panels are parallel to the direction of motion of the GMC. The GMC is shown with grey shades based on the surface density of a GMC with  $a_n = 5.8 a_c$ . The time with respect to the moment of encounter is indicated in each panel of the top row, where  $t_{\text{enc}} \equiv p/V_{\max}$ . The snapshots are taken in the centre-of-mass frame of the cluster and the viewing distance is  $60 a_c$ .

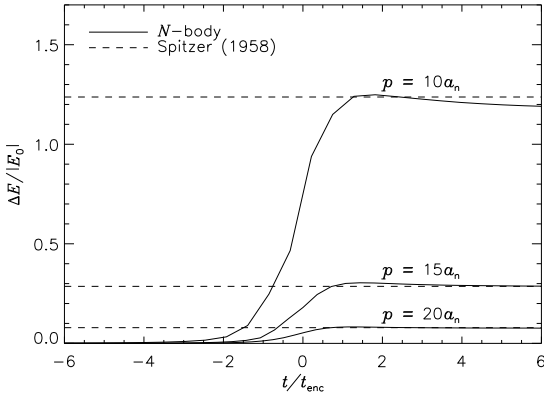


**Figure 5.** The evolution of the energy gain of a cluster during distant cloud encounters (full lines) with  $M_n = 2 \times 10^5 M_\odot$ ,  $V_{\max} = 30 \sigma_{\text{rms}}$  and three different impact parameter  $p$ . The dashed lines indicate the final energy gains predicted by S58 (Eq. 5).

#### 4.5 Relation between predicted energy gain and mass loss

In the previous section we found good agreement between the  $N$ -body simulations and our analytical formula for  $\Delta E/|E_0|$  of a cluster due to encounters with GMCs with different  $p$  and  $V_{\max}$  as long as  $\Delta E/|E_0| < 1$  (see Eq. 14). In Fig. 8 we show that deviations occur whenever the energy gain is larger than the initial cluster energy. We did a few more simulations of head-on encounters with higher GMC masses and compare all the predicted energy gains to the results from the simulations. The results are shown in Fig. 9. A one-to-one relation (dashed line) holds until  $\Delta E/|E_0| \simeq 5$ .

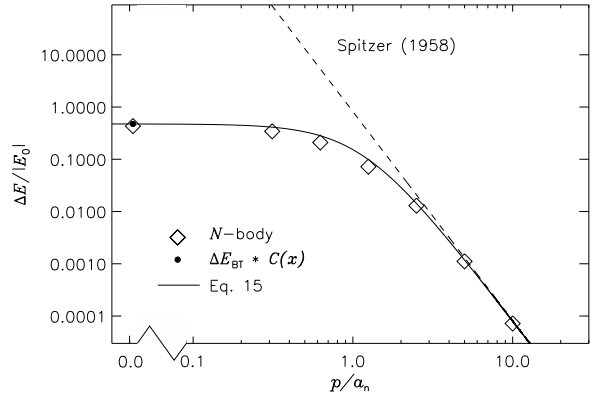


**Figure 7.** Fractional energy gain of a cluster as a function of the impact parameter  $p$  and for  $V_{\max} = 40 \sigma_{\text{rms}}$ . The results of the  $N$ -body simulations are shown with diamonds. The analytical result for head-on encounters, including the correction for the radius of the GMC is shown with a filled circle (left). The result for distant encounters from S58 is shown with the dashed line. The result from the interpolation between the two analytical predictions (e.g. Eq. 5 and 12), i.e. Eq. 14, is shown with the full line.

A simple functional ( $y = x[1 - \exp(-12/x)]$ ), which starts to deviate from a one to one relation around  $y \simeq 5$  and levels off at  $y = 12$  is also shown in Fig. 9 and describes the results well.

To derive a realistic disruption time of clusters due to encounters with GMCs, we need to know how the energy gain relates to the number of stars, or mass, that is lost from the cluster in the different encounters. In Fig. 10 we show the fractional mass loss ( $\Delta M/M_0$ ) as a function of  $\Delta E/|E_0|$ . The dashed line indicates a one-to-one relation and the full



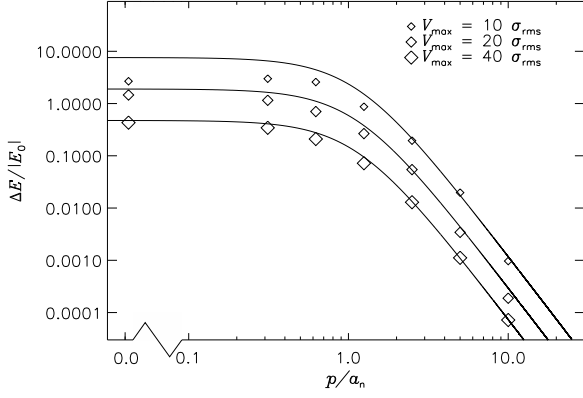


**Figure 8.** Fractional energy gain of a cluster as a function of the impact parameter  $p$  in units of  $a_n$  and for different values of  $V_{\max}$ . The results of the  $N$ -body simulations are shown with diamonds, where the size of the diamonds corresponds to the encounter velocity. The analytical results from Eq. 14 are shown with the full lines.

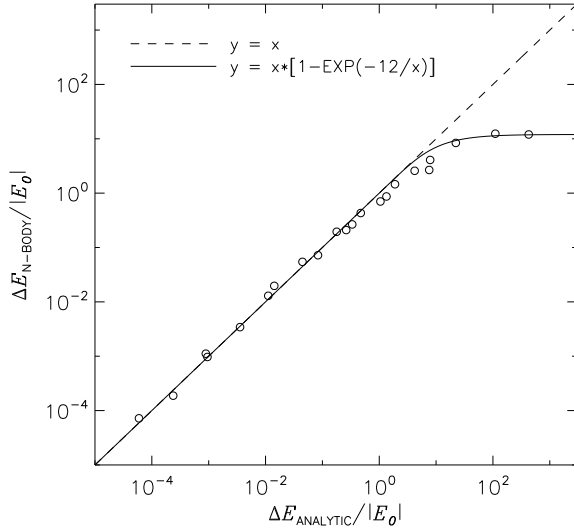


**Figure 9.** Relation between the fractional energy gain from the simulations and the analytical prediction of Eq. 14 (circles). A one-to-one relation is overplotted as the dashed line. A simple functional form, describing a linear function that saturates at a value of 12, fits the result at the high energy part well.

line is a fit to the results. The grey areas indicate the regions where  $\Delta M/M_0$  cannot be defined, since the cluster can not loose less than one star (i.e.  $M_0/2048$ , lower region), and it can not loose more than the total initial cluster mass (i.e.  $M_0$ , upper region). The fit shows an almost linear relation, where  $\Delta M/M_0$  is a fraction  $f = 0.22$  of  $\Delta E/|E_0|$ . Given the good agreement between the predicted energy gain and the one from the simulations, we can conclude that a fraction  $f = 0.22$  of the input energy is used to unbind stars. This implies that a fraction  $(1 - f)$  of  $\Delta E/|E_0|$  went into the velocity of the escaping stars, so that these have escaped with velocities much higher than the local escape velocity. Combined with the saturation of Fig. 9, this shows that

some encounters with  $\Delta E \gtrsim 10 E_0$ , called overkill encounters (Wielen 1985, 1988), can completely disrupt a cluster. We will further discuss this topic in § 5.3.

Since we consider isolated clusters, one might argue that there can be stars that have remained bound, but that would have been pushed over the tidal radius if the cluster was located in a galaxy. Assuming a disk galaxy with a flat rotation curve, with rotational velocity of  $V_0 = 220 \text{ km s}^{-1}$ , the tidal radius of a cluster depends then on its mass and galactocentric distance ( $R$ ) as  $r_t = (GM_c/2V_0^2)^{1/3} R^{2/3}$ . The estimated values of  $r_t$  for our cluster at  $R = [0.5, 1, 2] \times R_0$ , where  $R_0 = 8.5 \text{ kpc}$ , i.e. the solar neighbourhood, are  $r_t \simeq [13.8, 21.8, 34.6] \text{ pc}$ , respectively. We counted for our simulations the number of extra stars ( $\Delta N/N_0$ ) which after the encounter beyond these three radii. There is a linear relation between  $\Delta N/N_0$  and  $\Delta M/M_0$ , where the ratio of the two quantities is  $[1.3, 1.1, 1.0]$  for the three different tidal limits, respectively. So the effective value of  $f$  is somewhat higher when we take into account the tidal limit of the cluster. For the solar neighbourhood a good estimate would be  $f = 0.22 \times 1.1 \simeq 0.25$ . For clusters in the centres of galaxies the tidal radius is small and  $f$  can be a factor  $\sim 1.5$  higher. From now on we will assume a linear relation  $\Delta E/|E_0| = f \Delta M/M_0$ , with  $\simeq 0.25$ , which takes into account stars that have become unbound in isolation and/or are pushed over the tidal limit. This will be used in § 5 to derive the mass loss of clusters in environment with GMCs and the resulting cluster disruption time.

Hitherto, the cluster disruption time has always been defined as the time needed to bring the cluster energy to zero by periodically injecting energy with shocks (e.g. Ostriker et al. (1972) for the disruption time by disk shocks and Spitzer & Chevalier (1973) for the disruption by GMCs). We have shown that this overestimates the disruption time by a factor of  $1/f \simeq 4$ . A more accurate disruption time, taking into account this factor  $f$  is derived in the following section.

## 5 CLUSTER DISRUPTION TIME DUE TO ENCOUNTERS WITH GMCS

With the description of the mass loss from a cluster due to different types of encounters with GMCs of §§ 3,4 we can derive the disruption time of star clusters in an environment with GMCs, such as the solar neighbourhood.

### 5.1 Clusters in an environment with GMCs

When considering a distribution of GMCs and clusters with a relative velocity dispersion  $\sigma_{\text{cn}} = \sqrt{\sigma_n^2 + \sigma_c^2}$ , the probability of a relative velocity in the range  $v_0, v_0 + dv_0$  can be expressed as (BT87, Eq. 7-60)

$$dP = \frac{4\pi v_0^2}{(4\pi\sigma_{\text{cn}}^2)^{3/2}} \exp\left(-\frac{v_0^2}{4\sigma_{\text{cn}}^2}\right) dv_0. \quad (16)$$

Assuming a spatially homogeneous distribution of GMCs, the rate of encounters in the range  $b, b + db$  is then

$$\dot{C} = n_{\text{clouds}} v_0 2\pi b db dP \quad (17)$$

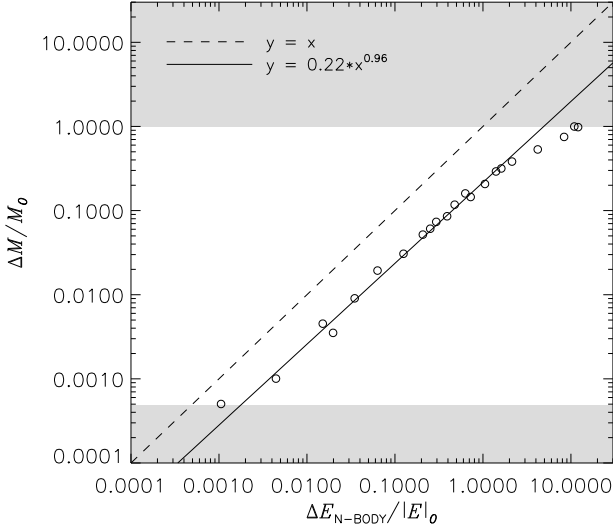


**Figure 10.** Relation between the fractional mass loss ( $\Delta M/M_0$ ) and the fractional energy gain ( $\Delta E/|E_0|$ ) for the simulations of § 4 (circles). The dashed line shows a one-to-one relation and the full line is a fit to the simulations. The grey areas indicate the regime where  $\Delta M/M_0$  can not be defined.

$$= \frac{n_{\text{clouds}} 8\pi^2 b db}{(4\pi\sigma_{\text{cn}}^2)^{3/2}} \exp\left(-\frac{v_0^2}{4\sigma_{\text{cn}}^2}\right) v_0^3 dv_0, \quad (18)$$

where  $n_{\text{clouds}}$  is the number density of clouds. The energy of the cluster increases at a rate

$$\dot{E} = \int_0^\infty \int_{b_{\text{min}}}^{b_{\text{max}}} \dot{C}(b, v_0) \Delta E(b, v_0) db dv_0, \quad (19)$$

where  $\Delta E(b, v_0)$  follows from Eq. 14 after converting  $b$  and  $v_0$  to  $p$  and  $V_{\text{max}}$  due to gravitational focusing. This integral can be calculated numerically.

In Fig. 11 we illustrate this using the parameters for clusters and GMCs used in the  $N$ -body simulations of § 4, e.g.  $M_n = 10^5 M_\odot$ ,  $a_n = 6.8$  pc and  $\sqrt{r^2} \simeq 1.8$  pc. We assume that young clusters and GMCs have the same velocity dispersion, i.e.  $\sigma_n = \sigma_c = 7 \text{ km s}^{-1}$  (Stark 1984; Piskunov et al. 2006). The velocity dispersion of the motion of GMCs with respect to clusters, is then  $\sigma_{\text{cn}} = \sqrt{\sigma_n^2 + \sigma_c^2} \simeq 10 \text{ km s}^{-1}$ . In the left panel of Fig. 11 we show the impact rate  $\dot{C}$  of Eq. 18 in units of  $n_{\text{clouds}}$  as a function of  $b$  and  $v_0$ , in units of  $a_n$  and  $\sigma_{\text{cn}}$ , respectively. In the middle panel we show  $\Delta E/|E_0|$  for individual encounters as a function of  $b/a_n$  and  $v_0/\sigma_{\text{cn}}$ , where we have converted  $b$  and  $v_0$  to  $p$  and  $V_{\text{max}}$  first, and then substituted these values in the equation for energy gain (Eq. 14). The rate of energy gain as a function of  $b/a_n$  and  $v_0/\sigma_{\text{cn}}$  is the product of the encounter rate times the energy gain per encounter and is shown in the right panel. The isocontours indicate the regions where 10, 50 and 75% of the total energy per unit time is produced. This total energy was not determined from this graph, but from a numeric integration of a similar figure, but with an area that is 100 times bigger. Most of the energy is injected by fast ( $v_0/\sigma_{\text{cn}} \simeq 2$ ) and close ( $b/a_n \simeq 1$ ) encounters. The encounter velocities ( $V_{\text{max}}$ ) are even higher than  $2\sigma_{\text{cn}}$  due to gravitational focusing and this means that the impulse approximation is valid for these encounters. In § 4.4 we found

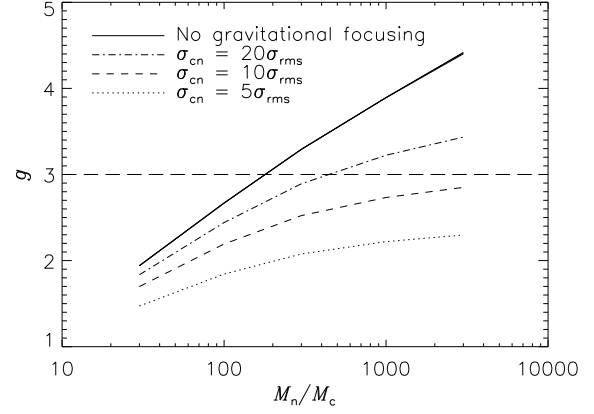


**Figure 12.** The correction factor  $g$  for close encounters (see text for details) as a function of GMC mass. The full line shows the result when gravitational focusing is ignored, and the other lines show the results for 3 different values of  $\sigma_{\text{cn}}$  when gravitational focusing is considered. The predicted value of  $g = 3$  of BT87 is indicated with the dashed horizontal line.

that the distant encounter regime of S58 holds for  $p \geq 5a_n$ . The peak in the right panel of Fig. 11 around  $b \simeq a_n$  illustrates that the approximations of S58 for a point source GMC are not applicable for the encounters that inject the majority of the energy. In that regime it is important to use the more accurate description for the energy gain found in § 3.3 (Eq. 14).

BT87 solved Eq. 19 by substituting the energy gain for distant encounters of S58. They then integrate  $b$  from  $R_n$  to infinity and correct for the missing close encounters with a factor  $g$  of order unity. The advantage of this solution is that the result has  $R_n^2$  in the denominator, which can be combined with  $M_n$  and  $n_{\text{clouds}}$  to express the final result in the observable molecular gas density ( $\rho_n$ ) and surface density of individual GMCs ( $\Sigma_n$ ). Our results allow us to quantify the parameter  $g$  of BT87 by integrating Eq. 19 numerically from 0 to infinity and from  $R_n$  to infinity. When gravitational focusing is ignored, the value of  $g$  depends only on  $M_n$ , since in that case  $p = b$  and  $V_{\text{max}} = v_0$ . Including gravitational focusing makes  $g$  dependent on  $\sigma_{\text{cn}}$  as well, since then encounters with initial  $b > R_n$  can result in  $p < R_n$ . Intuitively one thinks that the inclusion of gravitational focusing will increase the value of  $g$ , since there are more encounters with  $p < R_n$  to correct for. However, the encounter velocity  $V_{\text{max}}$  is always higher than  $v_0$ , which will make the energy gain of the cluster for these encounters lower. In Fig. 12 we show the resulting  $g$  for various values of  $M_n$  ignoring gravitational focusing (full line) and for three values of  $\sigma_{\text{cn}}$ . The horizontal dashed line indicates the estimated value of BT87 for  $g$ . For the solar neighbourhood (e.g.  $M_n \simeq 10^5 M_\odot$ ,  $\sigma_{\text{cn}} \simeq 10 \text{ km s}^{-1}$ ) our results show that  $g \simeq 2.5$ , slightly lower than predicted by BT87.

Using the relation between energy gain and mass loss of § 4.5 we can define the mass loss rate of the cluster as

$$\dot{M}_c = f \frac{\dot{E}}{E} M_c, \quad (20)$$

where  $f = 0.25$  is a dimensionless constant that relates fractional energy gain to fractional mass loss (see Fig. 10 and

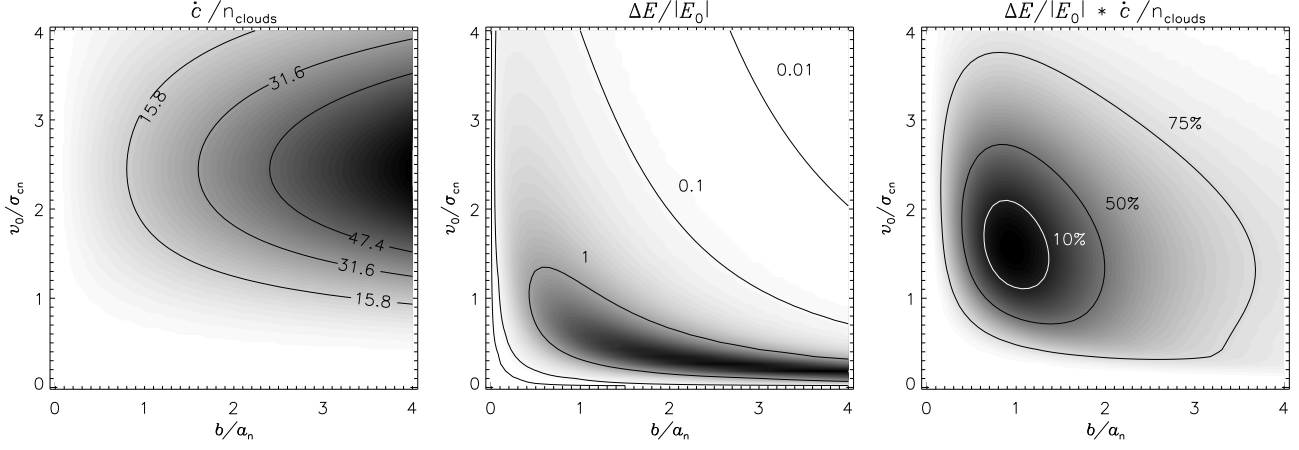


**Figure 11.** *Left:* The encounter rate ( $\dot{C}$ , Eq. 18), relative to  $n_{\text{clouds}}$ , for different values of  $b$  and  $v_0$ . *Middle:* Fractional energy gain (Eq. 14) for encounters with different  $b$  and  $v_0$ . *Right:* Rate of energy increase, resulting from the multiplication of  $\dot{C}$  and  $\Delta E$ .

§ 4.5). The initial cluster energy is  $E_0 = -\eta GM^2/(2r_h)$ , where  $\eta \simeq 0.4$ , depending on the cluster profile (Spitzer 1987).

We can derive a relation for the mass loss, using the expression for  $\dot{E}$  of BT87 (their Eq. 7-66), where we substitute  $\Sigma_n \equiv M_n/(\pi R_n^2)$ ,  $\rho_n \equiv M_n n_{\text{clouds}}$  and  $\dot{M} = f \dot{E}$

$$\dot{M}_c = \frac{8\pi^{3/2} g f}{3\sigma_{cn}\eta} G(\Sigma_n \rho_n) \left( \frac{r^2}{r_h^2} \right) r_h^3, \quad (21)$$

where the ratio  $(r^2/r_h^2)$  depends on the cluster model. For the Plummer cluster that we used  $(r^2/r_h^2) \simeq 4$  and for King profiles with dimensionless potential depth values of  $W_0 = [3, 5, 7, 9]$  it follows that  $(r^2/r_h^2) \simeq [1.5, 2, 3.5, 3.7]$ . From Eq. 21 we can derive the disruption time of clusters, by defining

$$t_{\text{dis}} = M_c/\dot{M}_c = \frac{3\sigma_{cn}\eta}{8\pi^{3/2} g f G} \left( \frac{1}{\Sigma_n \rho_n} \right) \left( \frac{r_h^2}{r^2} \right) \frac{M_c}{r_h^3}. \quad (22)$$

For the constants in Eq. 22 we have to make several assumption. First, we assume  $f = 0.25$ , as was found in § 4.5. For  $\sigma_{cn}$  we take  $10 \text{ km s}^{-1}$ , based on observations of GMCs in the solar neighbourhood (Stark & Brand 1989) and open clusters (Piskunov et al. 2006). For the cluster profile we assume a King profile with  $W_0 = 3$ , corresponding to  $c \equiv \log(r_t/r_c) \simeq 0.7$ , which is the mean concentration of the galactic open clusters (King 1962). King profiles are more realistic due to the tidal truncation, which the Plummer model does not have. For the  $W_0 = 3$  profile considered here,  $(r_h^2/r^2) \simeq 0.67$  and  $\eta = 0.42$  (BT87).

## 5.2 Dependence on the relation between cluster mass and radius

The solution for  $t_{\text{dis}}$  of Eq. 22 is very sensitive to the choice of  $r_h$ . Observations of (young) extra-galactic star clusters show that the projected half-light radius ( $r_{\text{eff}}$ ) of the majority of star clusters is confined to a narrow range of 2-4 pc (e.g. Bastian et al. 2005; Larsen 2004) and a very shallow relation between the radius and the mass. A factor of two difference in radius and nearly equal masses still results in

a factor of eight difference in  $t_{\text{dis}}$ . This implies that clusters that are a few times larger than the mean radius are very unlikely to survive and cluster that are a few times smaller will be almost insensitive to encounters by GMCs. We choose to use the recently observed relation between radius and mass of Larsen (2004), who fits a function of the form  $r_{\text{eff}} = A M_c^\lambda$  to a sample of young star clusters in nearby spiral galaxies and finds that  $A = 1.12 \pm 0.35$  and  $\lambda = 0.10 \pm 0.03$ . There is a large scatter around the fit relation, which, combined with the high sensitivity of  $t_{\text{dis}}$  on  $r_h$  (Eq. 22), makes it hard to relate mass to radius. However, since the relation of Larsen (2004) reflects the median relation between  $r_{\text{eff}}$  and  $M_c$ , the conversion will probably hold for a large cluster population. To convert  $r_{\text{eff}}$  to  $r_h$  we use the relation  $r_h = 4/3 r_{\text{eff}}$  (Spitzer 1987) and with that we can rewrite the result of Larsen (2004) as

$$r_h = 3.75 \left( \frac{M_c}{10^4 M_\odot} \right)^\lambda, \quad (23)$$

with  $\lambda \simeq 0.1$ . Substituting Eq. 23 in Eq. 22 and inserting all constants, yields an expression for the disruption time that is independent of  $r_h$  and depends on the assumed index that relates  $r_h$  and  $M_c$

$$t_{\text{dis}} = 2.0 \left( \frac{5.1 M_\odot^2 \text{ pc}^{-5}}{\Sigma_n \rho_n} \right) \left( \frac{M_c}{10^4 M_\odot} \right)^\gamma \text{ Gyr}, \quad (24)$$

with  $\gamma = 1 - 3\lambda$ . We normalised the product  $\Sigma_n \rho_n$  to the value for the solar neighbourhood ( $\Sigma_n = 170 M_\odot \text{ pc}^{-2}$  and  $\rho_n = 0.03 M_\odot \text{ pc}^{-3}$ , Solomon et al. 1987). When taking the 1 sigma upper bound value of  $\lambda \simeq 0.13$  from Larsen (2004), the index  $1 - 3\lambda = 0.61$  agrees very well with the value of 0.62 found from observations (Lamers et al. 2005) and from  $N$ -body simulations of clusters in the solar neighbourhood, dissolving under the combined effect of a tidal field, a realistic mass function and stellar evolution (Baumgardt & Makino 2003; Takahashi & Portegies Zwart 2000). These simulations adopted a slightly different relation between  $r_h$  and  $M_c$  since they assumed that at a given galactocentric distance the cluster size scales with the tidal radius ( $r_h \propto M_c^{1/3}$ ). The multiplicative constant of Eq. 24 is a factor of about 7 higher than what was found from ear-

lier studies (e.g. S58; Spitzer & Chevalier 1973; BT87). The difference can largely be explained by our factor  $f \simeq 0.25$  from § 4.5, that relates energy gain to mass loss. The remaining difference is caused by the lower value we found for  $g$  and a slightly different value for the product  $\Sigma_n \rho_n$ .

### 5.3 Disruption by single encounters

In the derivation of  $t_{\text{dis}}$  in the previous sections we integrated over the full range of  $b$  and  $v_0$  in Eq. 19 to get an expression for the rate of energy gain of a cluster due to GMC encounters. Doing so, we implicitly assume that disruption is caused by a large number of encounters. However, if the cluster is completely disrupted by the first encounter with a GMC, Eq. 22 will overestimate  $t_{\text{dis}}$ . Fig. 10 shows that a single encounter can indeed disrupt the cluster (see also Wielen 1985 and Terlevich 1987). If cluster disruption was always caused by single encounters, then Eqs. 22&24 would overestimate the disruption time in all cases. The most accurate approach is to include the saturation function of Fig. 9 in the relation between energy gain and mass loss (Eq. 20), i.e. to exclude encounters with  $\Delta E \gtrsim 10 E_0$ . This results in  $\Delta M/M_0=1$  for  $\Delta E/|E_0| \gtrsim 10$ . However, this would not have allowed us to come to the convenient linear dependence of  $t_{\text{dis}}$  on  $\rho_n$  and  $\Sigma_{\text{mol}}$  in Eq. 22.

Alternatively, we here estimate the typical time scale for a cluster to be disrupted by one single encounter ( $t_{\text{dis}}^{\text{single}}$ ). Following Wielen (1985), we can calculate the critical encounter distance ( $p_{\text{crit}}$ ) for which one encounter will result in total disruption of the cluster. Based on Eq. 15, on the expression for the cluster energy  $|E_0| = \eta G M_c^2 / (2r_h)$  and on the relation between  $\Delta E/|E_0|$  and  $\Delta M/M_0$  from § 4.5 we can derive  $p_{\text{crit}}$  by solving for  $p$  in  $\Delta E/|E_0| = 1/f$ , such that

$$p_{\text{crit}}^2 = \left( \frac{8Gf}{3\eta} \frac{r^2}{r_h^2} \right)^{1/2} \frac{M_n}{V} \left( \frac{M_c}{r_h^3} \right)^{-1/2} - K. \quad (25)$$

In here  $K = \sqrt{r_h R_n^3}$ , which is the term in the denominator of Eq. 15 that makes  $\Delta E$  converge to the correct value for head-on encounters ( $p = 0$ ). Wielen (1985) did not include this term, since he assumed point-mass GMCs (Eq. 5). (Note that Eq. 15 is equal to Eq. 5 when  $K = 0$ ). The number of encounters with encounter parameter  $p$  depends on the GMC number density ( $n_{\text{clouds}}$ ) as

$$N = \pi p^2 n_{\text{clouds}} V \Delta t. \quad (26)$$

We can solve for  $\Delta t$  by setting  $N = 1$  and  $p = p_{\text{crit}}$ , which is then the time it takes for a disruptive encounter to occur

$$t_{\text{dis}}^{\text{single}} = \frac{1}{\pi p_{\text{crit}}^2 n_{\text{clouds}} V}. \quad (27)$$

In here gravitational focusing is ignored. Following Wielen (1985) and assuming point-mass GMCs, e.g.  $K = 0$ , we find an expression of  $t_{\text{dis}}^{\text{single}}$  of the form

$$t_{\text{dis}}^{\text{single}} = \left( \frac{3\eta}{8Gf\pi^2} \frac{r_h^2}{r^2} \right)^{1/2} \left( \frac{M_c}{r_h^3} \right)^{1/2} \frac{1}{\rho_n}, \quad (28)$$

where we have used  $\rho_n \equiv M_n n_{\text{clouds}}$  again. At first sight this relation for the disruption time looks similar to what we derived in the previous section (Eq. 22). The main difference is the scaling with the cluster density ( $M_c/r_h^3$ ). In

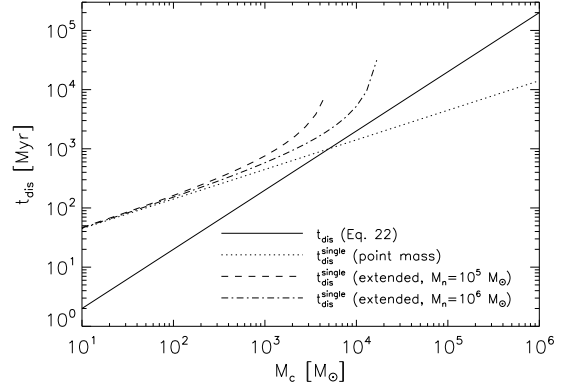


**Figure 13.** Comparison between  $t_{\text{dis}}$  of Eq. 22 (full line) and the single encounter disruption time ( $t_{\text{dis}}^{\text{single}}$ ). The dotted line shows the result of Wielen (1985) for point-mass GMCs and the dashed and dotted-dashed lines show the results for extended GMCs with  $M_n = 10^5 M_\odot$  and  $10^6 M_\odot$ , respectively.

Fig. 13 we show a comparison between  $t_{\text{dis}}^{\text{single}}$  of Eq. 28 (dotted line) and  $t_{\text{dis}}$  of Eq. 22 (full line) for different  $M_c$ . Here we used a constant  $r_h = 3.75$  pc and the same values for  $f, \eta$  and  $(r^2/r_h^2)$  as in § 5. The value of  $t_{\text{dis}}^{\text{single}}$  is smaller than the result of Eq. 24 for clusters with  $M_c > 5 \times 10^3 M_\odot$ . This implies that for massive clusters the life time is limited by the first disruptive encounter, rather than the successive heating by multiple encounters. For cluster of lower mass, the time it takes to disrupt by encounters with  $p > p_{\text{crit}}$  is shorter than  $t_{\text{dis}}^{\text{single}}$ . This mass dependence is counter intuitive at first, but is explained by the difference in scaling with  $M_c$  (Eqs. 22&28). Note that the crossing point (Fig. 13) does not depend on  $\rho_n$ , since Eqs. 22&28 depend in the same way on  $\rho_n$ .

In Fig. 13 we also plot the result of  $t_{\text{dis}}^{\text{single}}$  by substituting Eq. 25 with  $K = \sqrt{r_h R_n^3}$  in Eq. 27, based on  $M_n = 10^5 M_\odot$  (dashed line) and  $M_n = 10^6 M_\odot$  (dotted-dashed line) and Eq. 1. Here we use the same value for  $\rho_n$ , and then assume that all mass is in clouds with  $M_n = 10^5 M_\odot$  and  $10^6 M_\odot$ , respectively, to solve for  $n_{\text{clouds}}$  (Eq. 27). For low mass clusters, these solutions for  $t_{\text{dis}}^{\text{single}}$  agree with the result of Wielen (1985), since there  $p_{\text{crit}} \gtrsim \text{few } R_n$ , where the assumption of point-mass GMCs is valid (see Fig 7). For clusters with  $10^2 < M_c/M_\odot < 10^4$ , the solution for  $t_{\text{dis}}^{\text{single}}$  is higher than that of the point-mass assumption. This is because  $p_{\text{crit}}$  is smaller when extended GMCs are considered. In close encounters the extent of the GMC, e.g.  $K$ , is more important (Eq. 14). There is no solution for clusters with  $M_c > 5 - 10 \times 10^4 M_\odot$ , meaning that it is not possible to disrupt these clusters by a single encounters with a GMC with masses up to few times  $10^6 M_\odot$ .

The fact that the solutions for  $t_{\text{dis}}^{\text{single}}$  for realistic (extended) GMCs are always larger than  $t_{\text{dis}}$  from Eq. 22 justifies our assumptions of § 5.1. However, Fig. 13 shows that for a cluster with  $M_c = 10^{3-4} M_\odot$  the two solutions are close, meaning that clusters are destroyed by just a few encounters. This means that individual clusters will have strongly varying lifetimes. Our results of § 5 will, however, be valid as a statistical mean.

## 6 CONCLUSIONS AND DISCUSSION

We have derive an expression for the cluster disruption time ( $t_{\text{dis}}$ ) due to encounters with GMCs, based on the results of  $N$ -body simulations of different types of encounters between a cluster and a GMC. The expression for  $t_{\text{dis}}$  (Eq. 24) allows us to estimate the disruptive effect of GMCs in different environments and to compare it to other effects such as the galactic tidal field, stellar evolution and spiral arm shocks. From Eq. 24 we see that the disruption time for a  $10^4 M_{\odot}$  cluster in the solar neighbourhood is  $t_4 = 2.0$  Gyr. This is a factor of 3.5 shorter than what was found by Baumgardt & Makino (2003) for the combined effect of a realistic mass function, stellar evolution and the galactic tidal field ( $t_4 = 6.9$  Gyr). Note that the index  $\gamma$  is comparable, if we take the upper bound value of  $\lambda = 0.10 \pm 0.03$ , since Baumgardt & Makino (2003) found  $t_{\text{dis}} \propto [M_c / \ln(M_c)]^{0.75}$ . Lamers et al. (2005) showed that  $[M_c / \ln(M_c)]^{0.75} \propto M_c^{0.62}$ . The same mass dependence was also found from the age and mass distribution of cluster samples in different galaxies by Boutloukos & Lamers (2003) and from the age distribution of clusters in the solar neighbourhood by Lamers et al. (2005). For this last sample they found a shorter scaling value of  $t_4 = 1.3$  Gyr. Eq. 24 combined with the observed relation between  $r_h$  and  $M_c$  (Eq. 23) suggests that the combined mass loss by GMC encounters and evaporation in a tidal field preserves the index  $\gamma \simeq 0.62$ . A similar scaling between  $t_{\text{dis}}$  and  $M_c$  was found for the disruption time by spiral arm passages. The combination of all these effects and a comparison to the observed age distribution of open clusters in the solar neighbourhood will be discussed in more detail by Lamers & Gieles (2006).

The result of Eq. 24 can easily be applied to environments/galaxies with different molecular gas densities ( $\Sigma_{\text{mol}}$ ). The mid-plane density ( $\rho_n$ ) of GMCs scales with  $\Sigma_{\text{mol}}$  as  $\rho_n = \Sigma_{\text{mol}}/2h$ , where  $h$  is the vertical scale length of molecular gas, which is around 100 pc in the solar neighbourhood (Dame et al. 1987). Assuming that  $h$  is the same in M51, and therefore  $\rho_n = \Sigma_{\text{mol}}/200$  pc, we can predict  $t_4$  due to GMCs encounters once we know  $\Sigma_{\text{mol}}$  in M51 and compare this to the value of  $t_4$  for clusters in M51 (Gieles et al. 2005). Garcia-Burillo et al. (1993) find  $\Sigma_{\text{mol}} = 90 M_{\odot} \text{pc}^{-2}$  for the central region of M51, which is 14 times higher than in the solar neighbourhood (Solomon et al. 1987). This implies  $t_4 \simeq 2100 \text{ Myr}/14 = 150 \text{ Myr}$ . Note that this value is an upper limit, since we have assumed that the surface density of individual GMCs ( $\Sigma_n$ ) is independent of  $\Sigma_{\text{mol}}$ , while this could be higher in environments with higher  $\Sigma_{\text{mol}}$ . In addition, the values of  $f$  and  $g$  in Eq. 22 will probably be higher in the centre of M51 (see § 4.5 and § 5), which will make  $t_{\text{dis}}$  shorter. Also, we have assumed the same density profile as for the Galactic open cluster, e.g.  $W_0 = 3$ . A density profile of  $W_0 = 7$ , as found for the Galactic globular clusters, would reduce  $t_{\text{dis}}$  by a factor of two (Eq. 5). The resulting value of  $t_4$ , however, is very close to the value of  $t_4 = 100 - 200 \text{ Myr}$ , determined observationally by Gieles et al. (2005) from the age and mass distribution of star clusters in M51. Based on this work we think that we can explain the short disruption times of clusters in the centre of M51, if GMC encounters are the dominant disruption effect.

## ACKNOWLEDGEMENT

We thank the referee, Roland Wielen, for useful comments and pointing us to the problem of single disruptive encounters (§ 5.3). We enjoyed discussions with Nate Bastian, Søren Larsen and Sverre Aarseth. This work was done with financial support of the Royal Netherlands Academy of Arts and Sciences (KNAW), the Dutch Research School for Astrophysics (NOVA, grant 10.10.1.11 to HJGLM Lamers) and the Netherlands Organisation for Scientific Research (NWO, grant 635.000.001). The simulations were done on the MoDeStA platform in Amsterdam. MG thanks the Sterrekundig Instituut “Anton Pannekoek” of the University of Amsterdam for their hospitality during many pleasant visits.

## REFERENCES

- Aguilar L. A., White S. D. M., 1985, *ApJ*, 295, 374
- Bastian N., Gieles M., Lamers H. J. G. L. M., Scheepmaker R. A., de Grijs R., 2005, *A&A*, 431, 905
- Baumgardt H., Makino J., 2003, *MNRAS*, 340, 227
- Binney J., Tremaine S., 1987, *Galactic dynamics*. Princeton, NJ, Princeton University Press, 1987
- Boutloukos S. G., Lamers H. J. G. L. M., 2003, *MNRAS*, 338, 1717
- Chernoff D. F., Weinberg M. D., 1990, *ApJ*, 351, 121
- Dame T. M., Ungerechts H., Cohen R. S., de Geus E. J., Grenier I. A., May J., Murphy D. C., Nyman L.-A., Thaddeus P., 1987, *ApJ*, 322, 706
- de Grijs R., Anders P., 2006, *MNRAS*, 366, 295
- Garcia-Burillo S., Guelin M., Cernicharo J., 1993, *A&A*, 274, 123
- Gieles M., Athanassoula E., Portegies Zwart S. F., 2006, *MNRAS*, submitted
- Gieles M., Bastian N., Lamers H. J. G. L. M., Mout J. N., 2005, *A&A*, 441, 949
- Gnedin O. Y., Ostriker J. P., 1997, *ApJ*, 474, 223
- Heggie D. C., Mathieu R. D., 1986, *LNP Vol. 267: The Use of Supercomputers in Stellar Dynamics*, 267, 233
- Hodge P., 1988, *PASP*, 100, 576
- King I., 1962, *AJ*, 67, 471
- Kroupa P., 2001, *MNRAS*, 322, 231
- Lamers H. J. G. L. M., Gieles M., 2006, *A&A*, accepted
- Lamers H. J. G. L. M., Gieles M., Bastian N., Baumgardt H., Kharchenko N. V., Portegies Zwart S., 2005, *A&A*, 441, 117
- Lamers H. J. G. L. M., Gieles M., Portegies Zwart S. F., 2005, *A&A*, 429, 173
- Larsen S. S., 2004, *A&A*, 416, 537
- Makino J., Fukushige T., Koga M., Namura K., 2003, *PASJ*, 55, 1163
- McMillan S. L. W., Hut P., 1996, *ApJ*, 467, 348
- Oort J. H., 1958, *Ricerche Astronomiche*, 5, 507
- Ostriker J. P., Spitzer L. J., Chevalier R. A., 1972, *ApJ*, 176, L51+
- Piskunov A. E., Kharchenko N. V., Röser S., Schilbach E., Scholz R.-D., 2006, *A&A*, 445, 545
- Plummer H. C., 1911, *MNRAS*, 71, 460
- Portegies Zwart S. F., Hut P., Makino J., McMillan S. L. W., 1998, *A&A*, 337, 363
- Portegies Zwart S. F., Makino J., McMillan S. L. W., Hut P., 2002, *ApJ*, 565, 265

- Portegies Zwart S. F., McMillan S. L. W., Hut P., Makino J., 2001, MNRAS, 321, 199
- Solomon P. M., Rivolo A. R., Barrett J., Yahil A., 1987, ApJ, 319, 730
- Spitzer L., 1987, Dynamical evolution of globular clusters. Princeton, NJ, Princeton University Press, 1987, 191 p.
- Spitzer L. J., 1958, ApJ, 127, 17
- Spitzer L. J., Chevalier R. A., 1973, ApJ, 183, 565
- Stark A. A., 1984, ApJ, 281, 624
- Stark A. A., Brand J., 1989, ApJ, 339, 763
- Takahashi K., Portegies Zwart S. F., 2000, ApJ, 535, 759
- Terlevich E., 1987, MNRAS, 224, 193
- Theuns T., 1991, Memorie della Societa Astronomica Italiana, 62, 909
- Wielen R., 1971, A&A, 13, 309
- Wielen R., 1985, in Goodman J., Hut P., eds, IAU Symp. 113: Dynamics of Star Clusters Dynamics of open star clusters. pp 449–460
- Wielen R., 1988, in Grindlay J. E., Philip A. G. D., eds, IAU Symp. 126: The Harlow-Shapley Symposium on Globular Cluster Systems in Galaxies Dissolution of star clusters in galaxies. pp 393–406